NPS-69FU76101

NAVAL POSTGRADUATE SCHOOL

Monterey, California

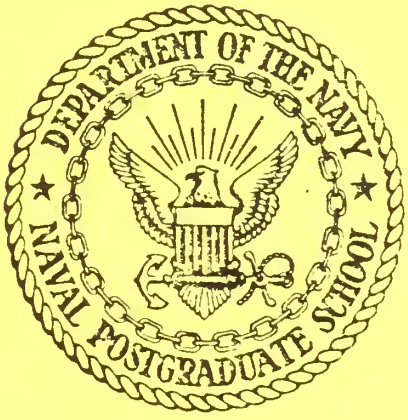

PHASE DISTORTION DUE TO AIRFLOW OVER
A HEMISPHERICAL LASER TURRET

by

A. E. Fuhs and S. E. Fuhs

September 1976

NAVAL POSTGRADUATE SCHOOL
Monterey, California

Rear Admiral Isham Linder
Superintendent

J. R. Borsting
Provost

PHASE DISTORTION DUE TO AIRFLOW OVER A HEMISPHERICAL LASER TURRET

Compressible flow over a laser turret creates a phase distortion. To gain insight to this problem a model of a hemispherical turret is developed. The flow field is obtained using a second order solution based on Janzen-Rayleigh expansion for the compressible potential flow equation. Contours of constant phase distortion were calculated; results at the critical Mach number are presented and discussed. It was found that the distortion at 0° elevation angle was equivalent to a positive lens whereas at 90° the distortion is similar to a negative lens. At 45° the main effect is beam tilting into the wind. For a ratio of beam radius to turret radius equal to 0.5, the focal length at beam elevation angle of 0°is 16.5 km. At beam elevation of 54° the beam tilt was found to be 26.5 microradians. The results of this paper are compared with other results reported in the literature.

UNCLASSIFIED

SECURITY CLASSIFICATION OF THIS PAGE *(When Data Entered)*

REPORT DOCUMENTATION PAGE		READ INSTRUCTIONS BEFORE COMPLETING FORM
1. REPORT NUMBER NPS-69FU76101	2. GOVT ACCESSION NO.	3. RECIPIENT'S CATALOG NUMBER
4. TITLE *(and Subtitle)* PHASE DISTORTION DUE TO AIRFLOW OVER A HEMISPHERICAL LASER TURRET		5. TYPE OF REPORT & PERIOD COVERED 6. PERFORMING ORG. REPORT NUMBER
7. AUTHOR(s) Allen E. Fuhs and Susan E. Fuhs		8. CONTRACT OR GRANT NUMBER(s)
9. PERFORMING ORGANIZATION NAME AND ADDRESS Distinguished Professor Allen E. Fuhs (Code 69Fu) Department of Mechanical Engineering Naval Postgraduate School		10. PROGRAM ELEMENT, PROJECT, TASK AREA & WORK UNIT NUMBERS
11. CONTROLLING OFFICE NAME AND ADDRESS		12. REPORT DATE September 1976 13. NUMBER OF PAGES
14. MONITORING AGENCY NAME & ADDRESS*(if different from Controlling Office)*		15. SECURITY CLASS. *(of this report)* Unclassified 15a. DECLASSIFICATION/DOWNGRADING SCHEDULE
16. DISTRIBUTION STATEMENT *(of this Report)* Approved for public release; distribution unlimited		
17. DISTRIBUTION STATEMENT *(of the abstract entered in Block 20, if different from Report)*		
18. SUPPLEMENTARY NOTES		
19. KEY WORDS *(Continue on reverse side if necessary and identify by block number)*		

20. ABSTRACT *(Continue on reverse side if necessary and identify by block number)*

Compressible flow over a laser turret creates a phase distortion. To gain insight to this problem a model of a hemispherical turret is developed. The flow field is obtained using a second order solution based on Janzen-Rayleigh expansion for the compressible potential flow equation. Contours of constant phase distortion were calculated; results at the critical Mach number are presented and discussed. It was found that the distortion at 0° elevation angle was equivalent to a positive lens whereas at 90° the distortion is similar to

DD FORM 1 JAN 73 1473 EDITION OF 1 NOV 65 IS OBSOLETE
S/N 0102-014-6601

UNCLASSIFIED

SECURITY CLASSIFICATION OF THIS PAGE *(When Data Entered)*

a negative lens. At 45° the main effect is beam tilting into the wind. For a ratio of beam radius to turret radius equal to 0.5, the focal length at beam elevation angle of 0° is 16.5km. At beam elevation of 54° the beam tilt was found to be 26.5 microradians. The results of this paper are compared with other results reported in the literature.

ABSTRACT

Compressible flow over a laser turret creates a phase distortion. To gain insight to this problem a model of a hemispherical turret is developed. The flow field is obtained using a second order solution based on Janzen-Rayleigh expansion for the compressible potential flow equation. Contours of constant phase distortion were calculated; results at the critical Mach number are presented and discussed. It was found that the distortion at 0° elevation angle was equivalent to a positive lens whereas at 90° the distortion is similar to a negative lens. At 45° the main effect is beam tilting into the wind. For a ratio of beam radius to turret radius equal to 0.5, the focal length at beam elevation angle of 0° is 16.5km. At beam elevation of 54° the beam tilt was found to be 26.5 microradians. The results of this paper are compared with other results reported in the literature.

ACKNOWLEDGMENT

This work was funded by the Air Force Weapons Laboratory. Monitors and sponsors of the work were Major Keith Gilbert, Dr. Barry Hogge and Captain Richard Cook. The senior author expresses his appreciation to the sponsors. They had an interest in the research, provided valuable suggestions and were a pleasure to work with.

It should be noted that the junior author of this report did all the programming of the computer.

PHASE DISTORTION DUE TO AIRFLOW OVER A HEMISPHERICAL LASER TURRET

by

A. E. Fuhs* and S. E. Fuhs**

I. INTRODUCTION

The index of refraction of air is related to mass density. Starting at modest subsonic Mach numbers, e.g. 0.3, and extending to transonic flight, flow over a blunt laser turret causes significant changes in density. The change in density, which in turn changes index of refraction, can defocus a laser beam.

Variable index of refraction within context of aeronautical applications is not a new problem; however, there are two aspects which are new. First, the laser beam is large relative to a characteristic turret dimension. Second, for many airborne applications the laser telescope requires a turret which protrudes into the flow.

Reconnaissance aircraft fly photographic missions. The compressible flow over the aircraft acts like a distorted lens and conceivably could cause distorted photographic images. The variable index of refraction is not a serious problem for reconnaissance aircraft for two reasons. The aperture of the camera is small compared to the characteristic scale of the distortions; in the case of a laser telescope this in not true. Furthermore, the camera on a reconnaissance aircraft is not mounted in a turret. To aim the camera the pilot aims the aircraft. Camera windows are flush with the aircraft surface.

Cruise missiles with intercontinental ranges may use celestial navigation which requires precise measurement of angular location of stars.

---

* Distinguished Professor of Mechanical Engineering

** Student, California Institute of Technology

A distorted lens created by the ambient flow field causes an error in measurement. Knowledge of the external aerodynamics is important.

A model which is useful for understanding the density field in the vicinity of a turret is the flow around a sphere or an ellipsoid. The plane containing an incoming fluid velocity vector and a diameter of the sphere does not have flow components normal to the plane. This is a plane of symmetry and conceptually can be considered a wall. The flow over the hemisphere above the plane can be calculated readily.

For incompressible flow, the solution for the flow over a sphere is well known. See for example pages 464-465 of Milne-Thompson,[1] pages 92-93 of Lamb[2] or pages 339-342 of Karamcheti.[3] Techniques are available to introduce the influence of compressibility or, stated another way, the influence of Mach number. One method is the Janzen-Rayleigh technique discussed briefly by Van Dyke.[4] Another brief description is given in Chapter 10 of Liepmann and Puckett.[5] The Janzen-Rayleigh method is discussed also on pages 328-334 of Oswatitsch.[6] Lord Rayleigh[7] provides the second order solution for a sphere in a paper published in 1916.

II. DISCUSSION OF ANALYTICAL MODELS

Optical distortion due to the external flow field can be divided into two categories. Viscous flow phenomena fall into one category and include shear layers, laminar and turbulent boundary layers, and shedding of discrete vortices. The other category involves the inviscid flow field. This paper treats the latter category.

Laser turrets can be classified as blunt or small-perturbation turrets. If the turret has a surface with a normal vector, $\vec{n}$, aligned parallel, or nearly so,to the freestream velocity vector, $\vec{V}$, the turret is "blunt". If the angle between the normal vectors of the turret surface and the freestream velocity vector are everywhere large, e.g. 60° to 90°, then the turret is "small-perturbation".

The turret being considered here is a hemisphere, which is obviously a blunt turret. At the front stagnation point of a hemispherical turret, $\vec{V} \cdot \vec{n} = -1.0$.

For a blunt turret, compressibility effects set in at a smaller freestream Mach number, M_∞. A useful concept is the critical Mach number, $M_\infty{}^*$. At the critical Mach number, somewhere on the body a <u>local</u> Mach number is just sonic. When $M_\infty > M_\infty{}^*$, the flow becomes inherently nonlinear and shock waves appear.

For a circular cylinder with its axis normal to the flow, the critical Mach number is 0.3985. For a sphere, the critical Mach number is 0.5868. A hemisphere-cylinder, which is oriented with the cylinder axis parallel to the freestream flow direction, has a critical Mach number less than 0.7. Hsieh[8] gives experimentally determined pressure coefficients for a hemisphere-cylinder over the Mach number range 0.7 to 1.0. In reference 9 Hsieh extends the Mach number range from 1.05 to 1.82. Using C_p

from reference 8, the maximum local Mach number is 1.25; the maximum local Mach number occurs at an angle of approximately 60° on the sphere. The angle is measured from the stagnation point to the location of minimum C_p.

For small perturbation turrets the critical Mach number is larger. Calculations were made of a turret on a cylindrical fuselage.[10] The turret shape was determined by

$$\left.\begin{aligned} R(x,\theta) &= R_0 + \frac{\varepsilon}{4}\left(1 + \cos\frac{\pi x}{\ell}\right)(1 + \cos f\theta) \\ R(x,\theta) &= R_0 \text{ for } \ell < |x| < L \text{ and } \pi/f < |\theta| < \pi \end{aligned}\right\} \qquad (1)$$

where R_0 is fuselage radius; ε, height of turret; ℓ, length of turret; $1/f$, the fraction of the 2π circumference occupied by the turret; and, L, the separation between periodic turrets. Table I summarizes the critical Mach number.

TABLE I. Critical Mach Numbers for Small-Perturbation Laser Turrets

ℓ/R_0	L/R_0	$1/f$	ε/R_0	M_∞*	maximum slope on turret
1.005	5.0	.333	0.05	.88	4.5°
			.10	.82	8.9°
			.15	.76	13.2°
			.20	.72	17.4°
			.25	.68	21.3°
			.30	.65	25.1°
			.35	.62	28.7°
			.40	.59	32.0°
			.45	—	35.1°
			.50	—	38.0°
			.55	—	40.7°

There are different analytical models that can be developed for laser turret geometries. Flow over blunt turrets can be determined using expansion techniques such as the Janzen-Rayleigh method mentioned earlier. As more terms in the expansion are evaluated, the more accurate are the flow field calculations as Mach number increases. Upper bound is the critical Mach number. For $M_\infty > M_\infty^*$, the calculations will be grossly in error.

There are numerical techniques which directly integrate appropriate differential equations. One method, which is applicable to axisymmetric flow, is the technique of South and Jameson.[11]

For small-perturbation laser turrets the equations can be linearized. Compressibility effects in subsonic or supersonic flow are incorporated. Transonic flow is excluded since the transonic equations are nonlinear even for small perturbation.

Figure 1 summarizes the regions in a body slope vs. Mach number map. The flow within the region ABCD can be described with sufficient accuracy using the linearized, small-perturbation equations. The line CD represents the critical Mach number. The line BC is shown at a slope of 30°. The assumptions involved in the linearization of the potential flow equation become less and less valid as the maximum slope increases. The region CDJ, which resembles an inverted triangle, requires solution of the nonlinear small-perturbation, transonic, potential equation.

The region EFGH defines the area where Janzen-Rayleigh technique is most useful. The line GH,which defines the critical Mach number, is shown dashed; the critical Mach number is a function of turret shape. Hence GH is intended to qualitatively suggest the upper bound for Mach number.

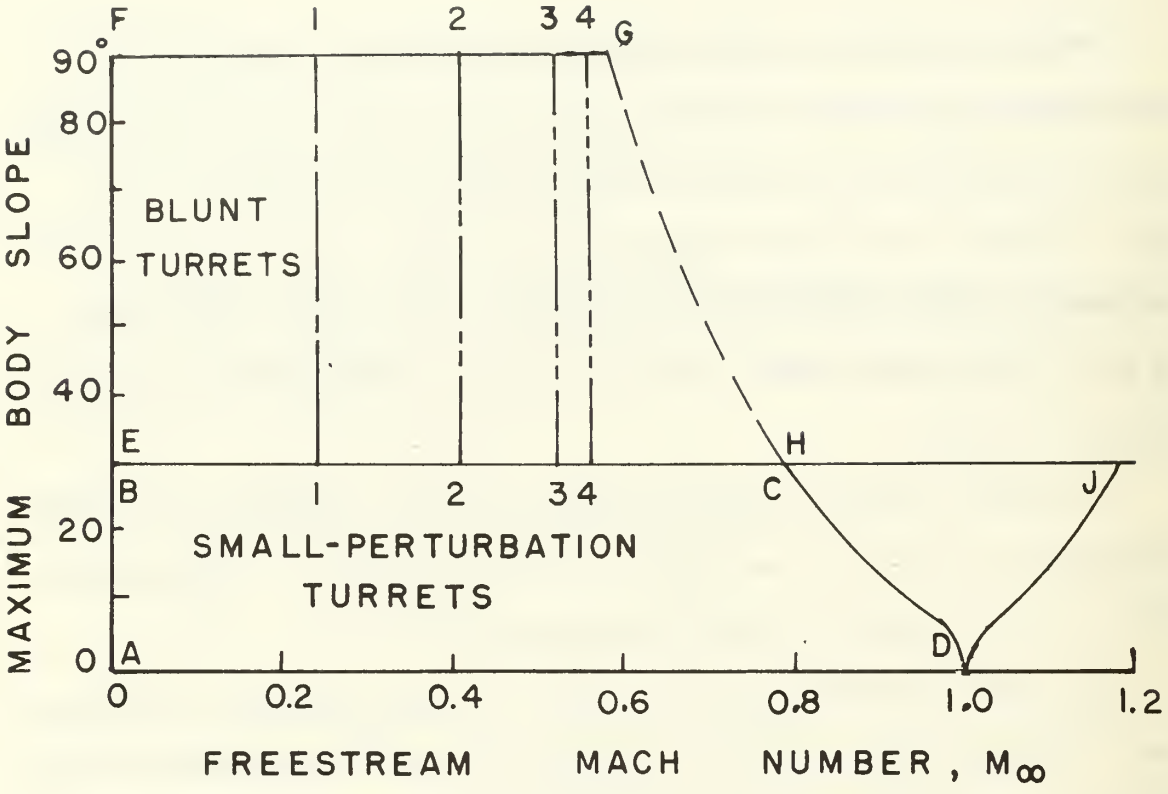

Figure 1. Freestream Mach Number Regions for Application of Various Analytical Models.

There are vertical lines 1, 2, 3, and 4 within region EFGH. These lines represent the upper bound of applicability of the first, second, third, and fourth order solutions when Janzen-Rayleigh technique is used. The first order solution may be applied within region F11E; the second order solution, within region F22E; etc.

A hemispherical turret considered in this paper is an example of a blunt turret falling along the line FG.

III. JANZEN-RAYLEIGH EXPANSION TECHNIQUE

In spherical coordinates, the equations of motion are as follows:

$$u \frac{\partial u}{\partial r} + \frac{v}{r} \frac{\partial u}{\partial \theta} - \frac{v^2}{r} = - \frac{1}{\rho} \frac{\partial p}{\partial r} = - \frac{a^2}{\rho} \frac{\partial \rho}{\partial r} \tag{2}$$

$$u \frac{\partial v}{\partial r} + \frac{v}{r} \frac{\partial v}{\partial \theta} + \frac{uv}{r} = - \frac{1}{\rho} \frac{1}{r} \frac{\partial p}{\partial \theta} = - \frac{a^2}{\rho r} \frac{\partial \rho}{\partial \theta} \tag{3}$$

$$\frac{1}{\rho} \left[u \frac{\partial \rho}{\partial r} + \frac{v}{r} \frac{\partial \rho}{\partial \theta} \right] + \frac{1}{r^2} \frac{\partial}{\partial r} (r^2 u) + \frac{1}{r \sin \theta} \frac{\partial}{\partial \theta} (v \sin \theta) = 0 \tag{4}$$

Equations (2) and (3) are Euler's equations. Equation (4) is the continuity equation. For flow over the sphere, there is no dependence on the azimuthal angle in polar coordinates. Consequently, equations (2) and (4) are two-dimensional equations depending only on r and θ.

Multiplying equation (2) by + u/a^2 and equation (3) by - v/a^2, adding and combining with equation (4) yields

$$\frac{1}{r^2} \frac{\partial}{\partial r} (r^2 u) + \frac{1}{r \sin \theta} \frac{\partial}{\partial \theta} (v \sin \theta) = \frac{1}{a^2} \left\{ u^2 \frac{\partial u}{\partial r} + \frac{uv}{r} \frac{\partial v}{\partial \theta} + uv \frac{\partial v}{\partial r} + \frac{v^2}{r} \frac{\partial v}{\partial \theta} \right\} \tag{5}$$

The speed of sound, a, is the local value and changes from point to point in the flow. It is necessary to account for variations in a. Using the energy equation along a streamtube, one can show that

$$\frac{a^2}{a_\infty^2} = 1 + \frac{\gamma - 1}{2} M_\infty^2 \left(1 - \frac{u^2 + v^2}{U^2} \right) \tag{6}$$

Inviscid flow is considered. A potential can be introduced for the velocity components

$$u = U \frac{\partial \phi}{\partial r} \tag{7}$$

$$v = \frac{U}{r} \frac{\partial \phi}{\partial \theta} \tag{8}$$

where U is the freestream velocity at upstream infinity. Introducing equations (7) and (8) into equations (5) and (6) yields equations in terms of a potential.

The Rayleigh-Janzen expansion considers the potential function to be given as

$$\phi = \phi_0 + M_\infty^2 \phi_1 + M_\infty^4 \phi_2 + \ldots \tag{9}$$

The solution for ϕ_0 is considered the first order solution. The solution involving both ϕ_0 and ϕ_1 is called the second order solution. In this paper only the second order solution is considered. For ease of writing, the following definition is introduced:

$$\psi = M_\infty^2 \phi_1 \tag{10}$$

To digress briefly from the development of the Janzen-Rayleigh expansion, the solution for the flow over a cylinder normal to the fluid velocity will be discussed. Van Dyke[4] indicates the solution for the cylinder has been performed to M_∞^{16}. For $\gamma = 7/5$, the result for maximum surface speed is

$$\frac{q_{max}}{U} = 2.00000 + 1.16667M_\infty^2 + 2.57833M_\infty^4 + \ldots\ldots + 25.59041M_\infty^8 + \ldots\ldots + 7450M_\infty^{16} \tag{11}$$

The critical Mach number for a cylinder is $M_\infty = 0.39852 \pm 0.00020$.

In terms of the potential function, the speed of sound becomes

$$\frac{a^2}{a_\infty^2} = 1 + M_\infty^2 F(\phi_r, \phi_\theta, r, \gamma) \tag{12a}$$

where F is given by

$$F = \frac{\gamma-1}{2} \left[1 - \left(\phi_r^2 + \frac{\phi_\theta^2}{r^2}\right)\right] \tag{12b}$$

With substitution of equations (9) and (10), the potential function becomes

$$\nabla^2\phi_0 + \nabla^2\psi = M_\infty^2 \left[\phi_r^2\,\phi_{rr} + \frac{2}{r^2}\,\phi_r\phi_\theta\phi_{\theta r} - \frac{1}{r^3}\,\phi_\theta^2\,\phi_r + \frac{1}{r^4}\,\phi_\theta^2\,\phi_{\theta\theta}\right] \tag{13}$$

where all terms on the right-hand side are determined from the first order potential function ϕ_0. The result of equating coefficients of like powers in M_∞^2 yields two equations

$$\nabla^2\phi_0 = 0 \tag{14}$$

and

$$\nabla^2\psi = M_\infty^2\,\nabla^2\phi_1 = M_\infty^2 \left[\phi_r^2\phi_{rr} + \frac{2}{r^2}\,\phi_r\phi_\theta\phi_{\theta r} - \frac{1}{r^3}\,\phi_\theta^2\,\phi_r + \frac{1}{r^4}\,\phi_\theta^2\,\phi_{\theta\theta}\right] \tag{15}$$

The right-hand side of equation (15) is known due to the fact that equation (14) can be solved to yield ϕ_0. To emphasize this fact, the first term on the right-hand side is written explicitly showing ϕ_0,

$$\phi_r^2\phi_{rr} = \left(\frac{\partial\phi_0}{\partial r}\right)^2 \frac{\partial^2\phi_0}{\partial r^2}$$

Equation (15) is Poisson's equation.

IV. FIRST ORDER SOLUTION

The first order solution is obtained from Milne-Thompson,[1] Lamb,[2] or Karamcheti.[3] It is

$$\phi_0(r, \theta) = U \left(r \cos \theta + \frac{R^3 \cos \theta}{2r^2}\right) \tag{16}$$

where R is the sphere radius. The upstream stagnation point, P, is at P(R, 180°); and the downstream stagnation point is at P(R, 0°). Using equation (16) one can determine the derivatives to substitute into equation (15). These are

$$\phi_r = U \cos \theta \left(1 - \frac{R^3}{r^3}\right) \tag{17}$$

$$\phi_{rr} = U \cos \theta \left[\frac{3R^3}{r^4}\right] \tag{18}$$

$$\phi_\theta = - r U \sin \theta \left[1 + \frac{1}{2} \frac{R^3}{r^3}\right] \tag{19}$$

$$\phi_{\theta\theta} = - r U \cos \theta \left[1 + \frac{1}{2} \frac{R^3}{r^3}\right] \tag{20}$$

$$\phi_{\theta r} = - U \sin \theta \left[1 - \frac{R^3}{r^3}\right] \tag{21}$$

The result of combining equations (15) and (17) to (21) is

$$\nabla^2 \phi_1 = \frac{\cos \theta}{r} \left\{3\lambda(1-\lambda)^2 + \sin^2 \theta \left[4 - \frac{9}{2} \lambda + 6\lambda^2 - \frac{17}{8} \lambda^3\right]\right\} \tag{22}$$

where $\lambda = R^3/r^3$ has been introduced.

Before proceeding with second order solution, a comment about boundary conditions is appropriate. The component of velocity normal to the surface of the sphere must be zero. At infinity, the velocity should be U. Consequently,

$$\left.\frac{\partial \phi_1}{\partial r}\right)_R = 0 \; ; \quad \left.\frac{\partial \phi_1}{\partial r}\right)_\infty = 0 \; ; \quad \left.\frac{1}{r} \frac{\partial \phi_1}{\partial \theta}\right)_\infty = 0 \tag{23}$$

Since ϕ_0 yields U at infinity, the velocity perturbation due to ϕ_1 should be zero at infinity.

V. RAYLEIGH SOLUTION FOR SECOND ORDER FUNCTION

In July, 1916, Lord Rayleigh[7] reported the solution for the second order function.

The Legendre functions

$$P_1 = \cos\theta \tag{24}$$

$$P_3 = \frac{5}{3}\cos^3\theta - \frac{3}{2}\cos\theta \tag{25}$$

are introduced into equation (15) in the following manner: First, equations (17) through (21) are substituted into equation (15); second, terms are grouped so as to form the functions P_1 and P_3. The result is

$$\nabla^2\phi_1 = \frac{U}{2}\left[\left(-\frac{36}{5}\frac{R^6}{r^7} + \frac{9}{2}\frac{R^9}{r^{10}}\right)P_1 + \left(6\frac{R^3}{r^4} - \frac{24}{5}\frac{R^6}{r^7} + \frac{3}{2}\frac{R^9}{r^{10}}\right)P_3\right] \tag{26}$$

Equation (26) is in the form

$$\nabla^2\phi_1 = \sum_n \sum_m r^{-m} P_n C_{nm} \tag{27}$$

where C_{1m} are zero except for m = 7 and 10; all C_{2m} are zero; and C_{3m} are zero except for m = 4, 7, and 10. Non-zero C_{nm} are the appropriate constants appearing in equation (26). The Legendre differential equation is

$$\frac{1}{\sin\theta}\frac{d}{d\theta}\left[\sin\theta\frac{dP_n}{d\theta}\right] + n(n+1)P_n = 0 \tag{28}$$

Define the function ϕ_{nm} which satisfies the equation

$$r^{-m}P_nC_{nm} = \nabla^2\phi_{nm} = \frac{\partial^2\phi_{nm}}{\partial r^2} + \frac{2}{r}\frac{\partial\phi_{nm}}{\partial r} + \frac{1}{r^2\sin\theta}\frac{\partial}{\partial\theta}\left[\sin\theta\frac{\partial\phi_{nm}}{\partial\theta}\right] \tag{29}$$

Assume

$$\phi_{nm} = r^{2-m}P_nA_{nm} \tag{30}$$

Consequently,

$$\frac{\partial \phi_{nm}}{\partial r} = (2-m)\, r^{1-m}\, P_n A_{nm} \tag{31}$$

and

$$\frac{\partial^2 \phi_{nm}}{\partial r^2} = (2-m)\,(1-m)\, r^{-m}\, P_n\, A_{nm} \tag{32}$$

Combining equations (29) and (32) gives

$$r^{-m} P_n\, C_{nm} = (2-m)\,(1-m)\, r^{-m}\, P_n\, A_{nm}$$

$$+ 2\,(2-m)\, r^{-m} P_n A_{nm} + \frac{r^{-m+2}}{r^2 \sin\theta}\, \frac{\partial}{\partial \theta} \left[\sin\theta\, \frac{\partial P_n}{\partial \theta} \right] A_{nm} \tag{33}$$

Substitution of equation (28) into equation (33) yields

$$r^{-m}\, P_n\, C_{nm} = A_{nm}\, r^{-m}\, P_n \left[(2-m)\,(1-m) + 2\,(2-m) - n\,(n+1) \right] \tag{34}$$

As a result

$$A_{nm} = \frac{C_{nm}}{(2-m)\,(3-m) - n\,(n+1)} \tag{35}$$

Using equations (26), (30), and (35), that part of the second order function identified as the particular solution is obtained

$$\phi_1 = U \left\{ P_1 \left[-\frac{R^6}{5r^5} + \frac{R^9}{24r^8} \right] + P_3 \left[-\frac{3R^3}{10r^2} - \frac{3R^6}{10r^5} + \frac{3R^9}{176r^8} \right] \right\} \tag{36}$$

The homogeneous solution is

$$\phi_1 = Ar\, P_1 + BP_1/r^2 + Cr^3 P_3 + D\, P_3/r^4 \tag{37}$$

At infinity the potential must be finite and the velocity must be U; the function ϕ_0 of equation (16) yields U. Consequently both A and C equal zero. At the surface of the sphere

$$\left.\frac{\partial \phi_1}{\partial r}\right)_{r=R} = 0 \qquad \text{and} \qquad \left.\frac{1}{r}\,\frac{\partial \phi_1}{\partial \theta}\right)_{\theta=0} = 0 \tag{38}$$

From the requirements of equation (38) combined with equations (36) and (37)

$$B = \frac{R^3}{3}\, U\, M_\infty^2 \tag{39}$$

and

$$D = \frac{27R^5U}{55}\, M_\infty^2 \tag{40}$$

The final expression for the potential function is

$$\phi = \phi_0 + M_\infty^2 \phi_1 = \left\{ U\left[r + \frac{R^3}{2r^2} \right] P_1 \right\} + UM_\infty^2 \left\{ \left[\frac{R^3}{3r^2} - \frac{R^6}{5r^5} + \frac{R^9}{24r^8} \right] P_1 + \left[-\frac{3R^3}{10r^2} + \frac{27R^5}{55r^4} - \frac{3R^6}{10r^5} + \frac{3R^9}{176r^8} \right] P_3 \right\} \tag{41}$$

The first term in brackets is ϕ_0; and the second, long term is the second order contribution.

VI. DEVELOPMENT OF PHASE DISTORTION

Use of Potential Function to Obtain Index of Refraction

The index of refraction and density are related by

$$n = 1 + \kappa' \frac{\rho}{\rho_\infty} \frac{\rho_\infty}{\rho_{SL}} = 1 + \kappa \frac{\rho}{\rho_\infty} \tag{42}$$

where κ' is a constant with value of about 2×10^{-4}. Note $\kappa = \kappa' \rho_\infty / \rho_{SL}$. The flow is assumed to be isentropic. Consequently

$$\frac{\rho}{\rho_\infty} = \left[\frac{1 + \frac{\gamma-1}{2} M_\infty^2}{1 + \frac{\gamma-1}{2} M^2} \right]^{\frac{1}{\gamma-1}} \tag{43}$$

The local Mach number is given by

$$M^2 = \frac{1}{a^2} \left[\left(\frac{\partial \phi}{\partial r} \right)^2 + \left(\frac{1}{r} \frac{\partial \phi}{\partial \theta} \right)^2 \right] \tag{44}$$

In equation (42) ρ is the local density, ρ_∞ is the freestream density, and ρ_{SL} is the sea level density on a standard day. By combining equations (6), (12a), (41), (42), (43), and (44), an expression is obtained for the index of refraction.

The turret has a characteristic length; for the sphere this is the radius R. The laser beam has a characteristic size which is the diameter D or radius R'. The wavelength of the laser radiation, λ, is also a characteristic length as will be demonstrated in subsequent discussion. Two nondimensional lengths can be formed. Since R occurs prominently in the equations for the potential, R is chosen as the reference length. With that choice, λ/R and D/R are two of the parameters specifying the problem.

Phase distortion is a function of the direction that the beam is pointed. Define e and a as elevation and azimuth angles. For the hemispherical turret, symmetry exists about the diameter of the sphere which is parallel to the freestream velocity vector. In general, two angles, e and a, are needed to define the beam direction; however, for the hemispherical turret only one angle is needed. Looking ahead, the angle θ' occurring in equations (45) and (46) will be used as the beam angle; see also Figure 2.

Geometrical Relations for Calculation of Phase Distortion

Figure 2 shows the geometry of the problem. The radius of the sphere is R. The beam is elevated at an angle θ'. The z axis is the same as the polar axis for polar coordinates.

To locate points within the beam, three variables are used; s is distance along the beam, as shown in Figure 3; α is an angle measured clockwise from the windward edge of beam; and R' is the radial distance from the beam centerline or axis.

The flow properties, i.e., density and local Mach number, are functions of r and θ. These are polar coordinates. Consequently, it is necessary to express r and θ in terms of θ', s, α, and R. The equations are

$$r^2 = \left[(R + s) \sin \theta' - R' \cos \alpha \cos \theta'\right]^2 + R'^2 \sin^2 \alpha + \left[(R + s) \cos \theta' + R' \cos \alpha \sin \theta'\right]^2 \qquad (45)$$

and

$$\theta = \tan^{-1} \frac{\sqrt{\left[(R + s) \sin \theta' - R' \cos \alpha \cos \theta'\right]^2 + R'^2 \sin^2 \alpha}}{\left[(R + s) \cos \theta' + R' \cos \alpha \sin \theta'\right]} \qquad (46)$$

Equations (45) and (46) can be used to evaluate equations (41) to (44).

The index of refraction is given by equation (42). Define N as the

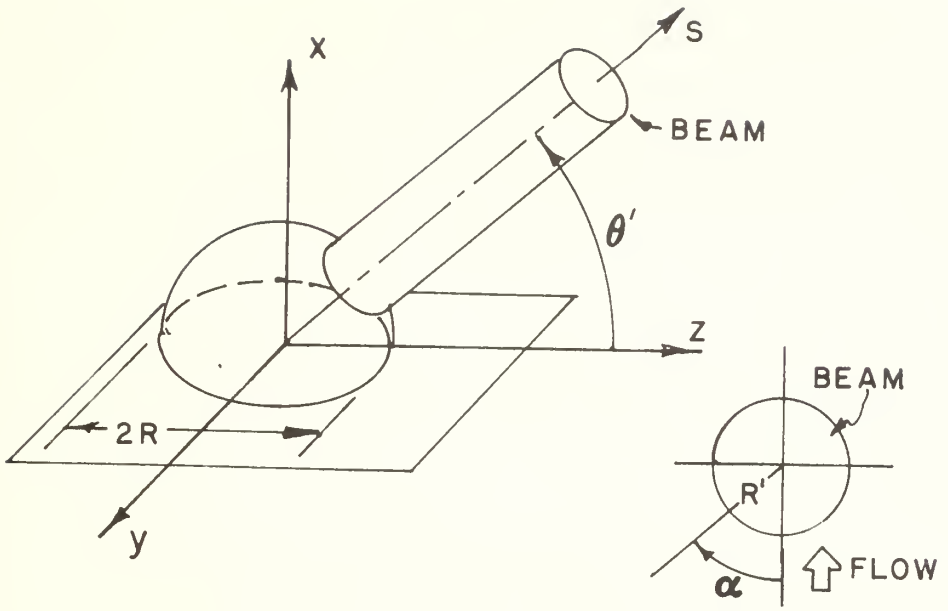

Figure 2. Geometry for Phase Distortion Calculation.

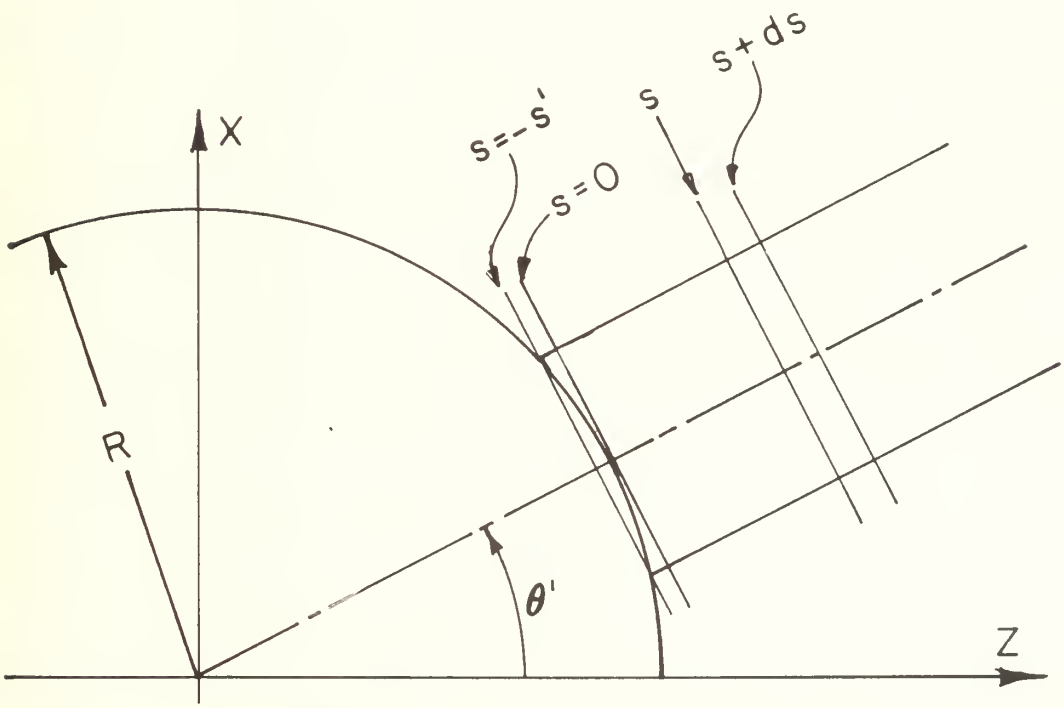

Figure 3. Cross Section of the Turret and Beam in the x-z Plane.

number of waves along a distance s. Hence

$$dN = \frac{ds}{\lambda} \tag{47}$$

where λ is the local wavelength. The local wavelength is a function of θ', α, R', and s. It is

$$\lambda = \frac{v}{f} = \frac{c}{nf} = \frac{c}{f(1 + \kappa\rho/\rho_\infty)} = \frac{\lambda_\infty(1 + \kappa)}{(1 + \kappa\rho/\rho_\infty)} \tag{48}$$

As a result, the number of waves is

$$N = \frac{1}{\lambda_\infty(1 + \kappa)} \int_{-s'}^{s} (1 + \kappa \frac{\rho}{\rho_\infty})ds \tag{49}$$

A reference is needed. The reference which is convenient is the number of waves along the beam axis; designate that quantity as N_0. Using this reference

$$N-N_0 = \frac{1}{\lambda_\infty(1+\kappa)} \left\{ \int_{-s'}^{s} (1+\kappa \frac{\rho}{\rho_\infty})ds - \int_{-s'}^{0} (1+\kappa\frac{\rho_r}{\rho_\infty})ds - \int_{0}^{s} (1+\kappa\frac{\rho_0}{\rho_\infty})ds \right\} \tag{50}$$

Note the density on the beam centerline for $-s' \leq s \leq 0$ is denoted by ρ_r, a reference density. For $0 \leq s < \infty$, the density on the centerline is ρ_0 which is a function of s. In equation (50) the value of unity in each integrand can be cancelled giving

$$N-N_0 = \frac{\kappa R}{\lambda_\infty(1+\kappa)} \left\{ \int_{0}^{s} \frac{\rho-\rho_0}{\rho_\infty} \frac{ds}{R} + \int_{-s'}^{0} \frac{\rho-\rho_r}{\rho_\infty} \frac{ds}{R} \right\} \tag{51}$$

The second integral in equation (51) has been termed the GAP INTEGRAL since it enters the equation as a result of the gap between s = -s' and s = 0. See Figure 3. In the calculations which were conducted, the gap

integral was evaluated by assuming $\rho_r = \rho_\infty$; this is an arbitrary assumption. Note that in equation (51) wavelength is nondimensionalized by R to form λ_∞/R. The distance along a ray is also nondimensional, i.e., ds/R.

A computer program has been developed for the HP9830 which calculates $N - N_0$ as a function of sphere radius, R; elevation angle, θ'; radius within the beam, R'; angle within the beam, α; freestream Mach number, M; wavelength, λ_∞; constant in density equation (42), κ'; ratio of heat capacities for air, γ; and freestream speed of sound, a_∞. Note that it is not necessary to specify ρ_∞ since all calculations depend on density ratio; see equations (48) and (51). Values used in the calculations are as follows:

$$R = 0.9144 \text{ meter}$$

$$\lambda_\infty = 3.8 \text{ micron} = 3.8 \times 10^{-6} \text{ meter}$$

$$\kappa' = 2 \times 10^{-4}$$

$$a = 342 \text{ meter/sec}$$

$$\gamma = 1.4$$

M_∞, R', α, and θ' have been varied. Calculations have been performed to the extent necessary to plot phase distortion maps.

VII. RESULTS OF CALCULATIONS

Graphical Presentation of Results

Plots of isocontours of phase shift were made for steps of 18° starting with $\theta' = 0$ to $\theta' = 90°$. The plots are shown in Figures 4 to 9. To avoid awkward decimal values, units of the plots are deci-wavelength; hence 250 is 2.5 wavelengths, and 25 is a quarter of a wavelength. Recall that the beam center line is used as reference for

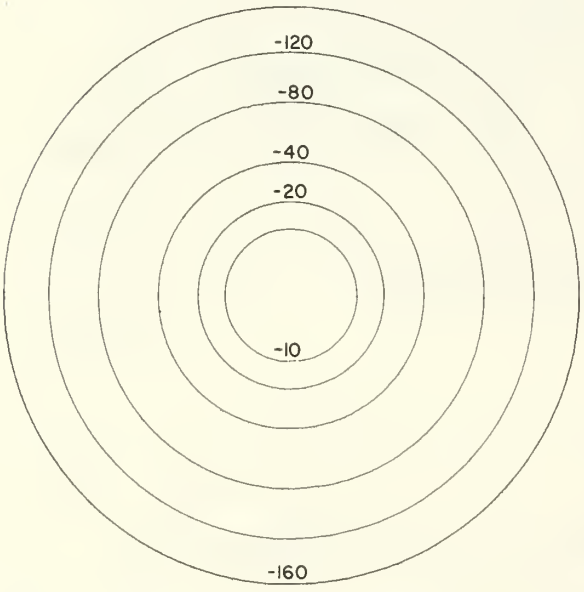

Figure 4. Contours of Constant Phase Shift for $\theta' = 0°$.

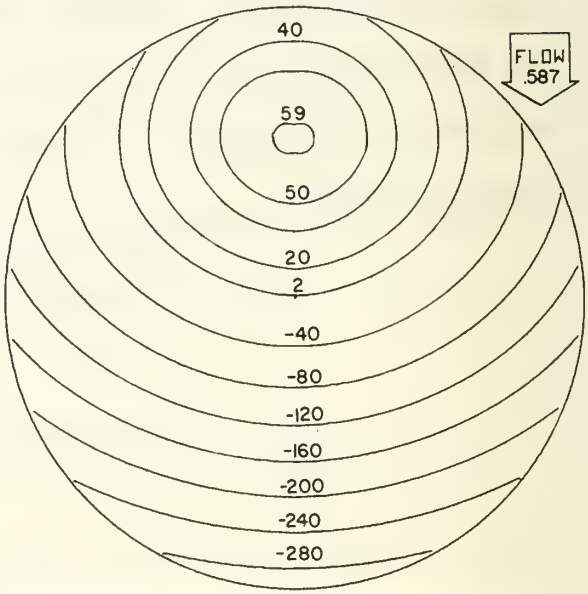

Figure 5. Contours of Constant Phase Shift for $\theta = 18°$.

the phase shift. Reference to equation (51) shows that a positive phase shift is the case of more waves along the ray in question than along the ray coincident with the beam centerline.

For the series of plots in Figures 4 to 9 the critical Mach number was selected. For a sphere this is $M_\infty^* = 0.587$. The gap integral is not included in the phase shift. The outer edge of each plot is for $D/2R = 0.5$. Recall that D = beam diameter, and R = turret radius.

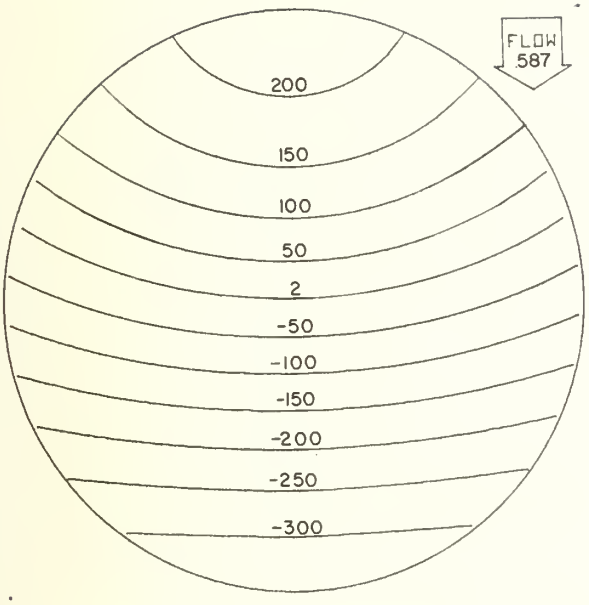

Figure 6. Contours of Constant Phase Shift for $\theta' = 36°$.

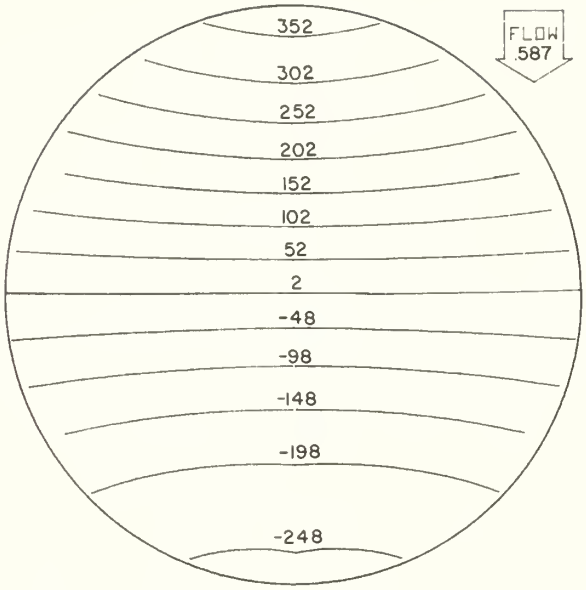

Figure 7. Contours of Constant Phase Shift for $\theta' = 54°$.

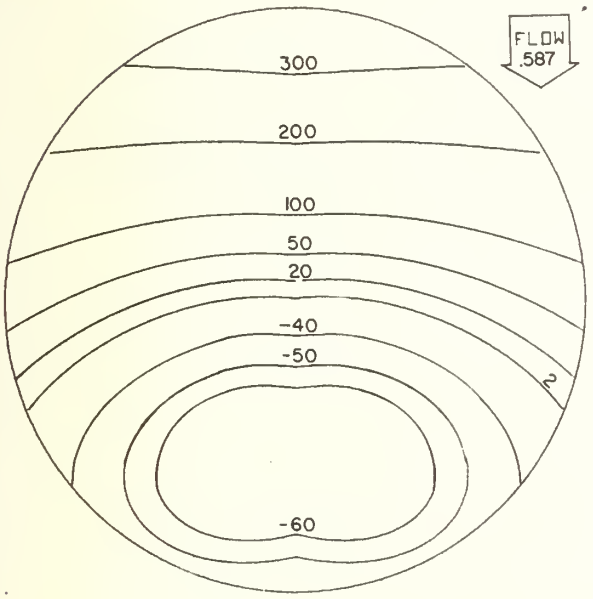

Figure 8. Contours of Constant Phase Shift for $\theta' = 72°$.

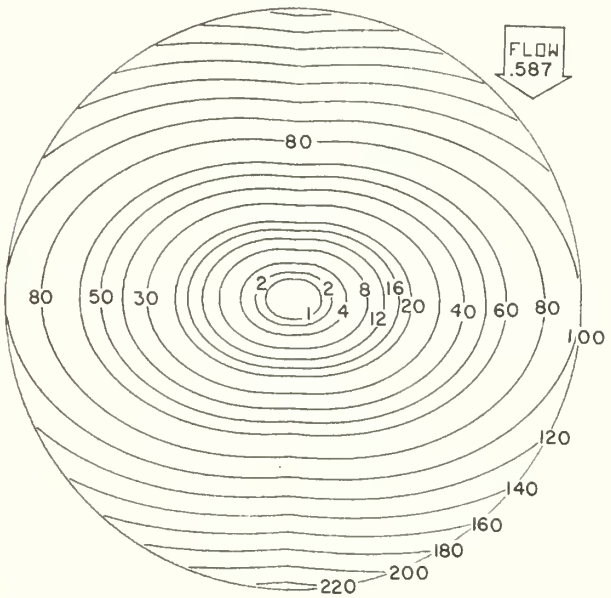

Figure 9. Contours of Constant Phase Shift for $\theta' = 90°$.

To provide insight to the magnitude of gap integral, Table II gives the maximum value for each of the plots.

TABLE II. MAXIMUM VALUE OF GAP INTEGRAL

beam elevation angle θ'	maximum value of gap integral in deciwave lengths and location within beam (gap integral)	α
0°	+ 36.8	*
18°	+ 65.4	0°
36°	+ 67.8	0°
54°	- 83.6	180°
72°	- 86.3	120°
90°	- 86.6	90°

M_∞ = 0.586 for these calculations. Also $D/2R$ = 0.5.

* not a function of α.

Evaluation of Phase Distortion as a Function of Distance Along the Beam

An important question is the rate of decay of the integrand in equation (51). Calculations were made of

$$\frac{\partial(N - N_0)}{\partial(s/R)}$$

which is the phase distortion per unit distance along the beam. The phase distortion per unit distance is a function of distance along the beam. Results of the calculation are shown in Figure 10. The phase distortion is the area enclosed by one of the curves. Most of the phase distortion occurs within a length equal to one turret radius.

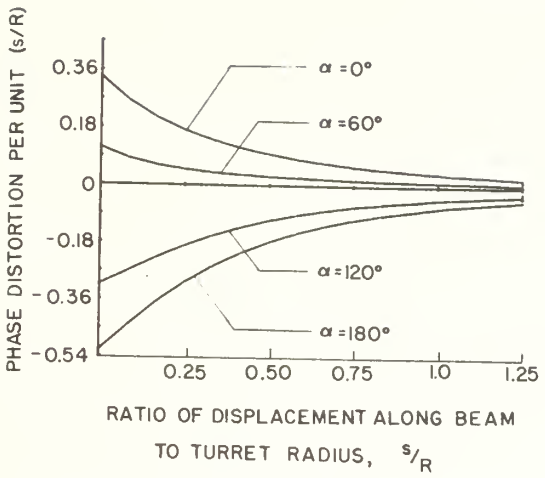

Figure 10. Phase Distortion Per Unit (s/R) as a Function of Distance Along the Beam for Rays at $\alpha = 0°$, 60°, 120°, and 180° Within the Beam. Elevation Angle was $\theta' = 18°$.

Dependence of Phase Distortion on Flight Mach Number

Another parameter of considerable interest is the dependence of phase distortion on Mach number. Qualitatively, isodensity contours at $M_\infty < M_\infty^*$ have an appearance the same as for $M_\infty = M_\infty^*$. Quantitatively, there are changes in both the shape of an isocontour of constant phase shift and the magnitude of the phase shift. Table III compares magnitudes of distinctive features of the maps for two Mach numbers. Table III should be studied simultaneously with the appropriate figure for θ'.

Phase distortion curves based solely on a first order calculation, i.e., using ϕ_0 in equation (9) only, should have the same shape for all M_∞. A calculation of phase distortion based on a second order solution, i.e., using both ϕ_0 and ϕ_1 in equation (9), should be a function of M_∞. Figure 11 shows the change in shape of a phase distortion curve with Mach number. The curves are drawn for $\theta' = 18°$; M_∞, either 0.300 or 0.587; R'/R from 0 to 0.5 and for $\alpha = 0°$ and $\alpha = 180°$. The phase distortion has been normalized with the value at R'/R = 0.5 and $\alpha = 180°$. Differences in the curves are due to Mach number effects.

TABLE III. COMPARISON OF MAGNITUDE OF PHASE SHIFT FOR TWO DIFFERENT MACH NUMBERS

θ'	feature of isocontour map	value at M_∞ = 0.300	M_∞ = 0.587
0°	maximum ϕ at beam edge	-41.5	-160
18°	maximum ϕ at positive peak	+15	+ 60
	minimum ϕ	-69.6	-290
36°	maximum ϕ	+44.2	+240
	minimum ϕ	-80.3	-345
54°	maximum ϕ	+85.2	+370
	minimum ϕ	-54.4	-268
72°	maximum ϕ	+83.7	+386
	minimum ϕ at negative valley	-14.1	- 74.1
90°	maximum ϕ at α = 0°	+49.1	+223

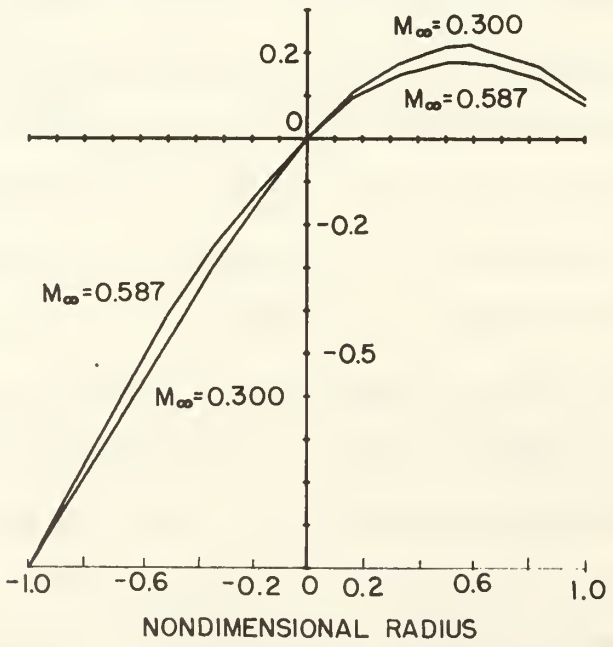

Figure 11. Phase Distortion for Two Mach Numbers.

Interpretation of Results

Phase shift for $\theta' = 0$ as shown in Figure 4 consists of a series of concentric circles. Since the phase shift is negative, the beam is being focused. Concentric curves with negative phase distortion gives a positive focus.

The contours of constant phase shift for $\theta' = 54°$ are almost straight lines. The algebraic signs of phase shift contours indicate the beam is being tilted in a direction opposite to the relative wind. The angular tilt is given roughly by

$$(\text{tilt angle}) = \left[(N-N_0)_{0°} - (N-N_0)_{180°}\right] \frac{\lambda_\infty}{2R'} \qquad (52)$$

Inserting the appropriate values (values for $N-N_0$ were obtained from Table III) gives

$$(\text{tilt angle}) = \frac{(370 + 268)\ (3.8 \times 10^{-6}\text{m})}{(2)\ (.4572\text{m})\ (100)} = 26.5 \text{ microradians}$$

Tilt of a beam does not cause a serious problem.

These results for tilt angle can be compared with similar work by Cook.[12]

Captain Cook[12] used the following values in a sample calculation (notation has been adjusted to match this report):

$R' = 0.25\text{m}$	$\lambda_\infty = 10.6$ micron
$R = 0.71\text{m}$	$\kappa'/\rho_\infty = 0.22\ \text{cm}^3/\text{gm}$
$M_\infty = 0.5$	$\kappa' = 2.7 \times 10^{-4}$

For $\theta' = 54°$, a beam tilt of 63 microradians was calculated. When adjustments are made for different parameters used to calculate the two results, i.e., 63 and 26.5 microradians, the answers agree quite favorably.

It is possible to determine an approximate focal length, F_α. The subscript, α, indicates the focal length in a plane defined by α of

Figure 2. The appropriate equation is

$$\frac{1}{F_\alpha} = \frac{\lambda_\infty}{(\Delta R')^2} \left[(N-N_0)_{R_2'} - 2(N-N_0)_{R_1'} \right] \tag{53}$$

Equation (53) was evaluated for $\alpha = 0$ and for the following values for other parameters

$\rho_\infty = 1.23 \times 10^{-3}$ gm/cm^3

$\lambda_\infty = 3.8 \times 10^{-6}$ m $\qquad$ $M_\infty = 0.587$

$\Delta R' = 0.1524$ m $\qquad$ $R = 0.9144$ m

$(N-N_0)$ at $R_2' = 0.799$ wavelengths

$(N-N_0)$ at $R_1' = 0.214$ wavelengths

$\theta' = 0°$

A focal length of 16.5 km was found.

Before proceeding, some additional information concerning equation (53) is appropriate. Equation (53) is a specialization of the equation

$$\frac{1}{F_x} = \frac{\partial^2 I}{\partial x^2} \tag{54}$$

where

$$I = \int_a^b n \, ds \tag{55}$$

For the problem at hand equations (54) and (55) yield

$$\frac{1}{F_x} = \frac{\kappa}{(\Delta x)^2} \left\{ \int \frac{\rho_2 - \rho_0}{\rho_\infty} ds - 2 \int \frac{\rho_1 - \rho_0}{\rho_\infty} ds + \int \frac{\rho_0 - \rho_0}{\rho_\infty} ds \right\} \tag{56}$$

where $\rho_2 = \rho(x_2)$, $\rho_1 = \rho(x_1)$, etc. It is obvious that the third integral is zero. Equation (56) leads to equation (53). From Cook's[12] report for the previously cited values for R, R', M_∞, etc., a focal length of about 6 km is calculated. Adjusting the value for values of R, R', M_∞, etc.,

used in the calculations of this report, good qualitative agreement is obtained.

Wolters and Laffay[13] have calculated focal length for an aperture of a turret on a F-15. The turret geometry was a cylinder with axis parallel to the freestream; radius of the cylinder was 0.5 m. When viewed from a position normal to the axis, a cylinder appears as a rectangle. The square corners were rounded with a radius of 0.3 m. Without rounding of the corners, the cylinder viewed from its end would appear as a disc with radius 0.5 m. With the rounding of the corners, the disc is reduced to 0.2 m; the disc is normal to the freestream velocity vector.

Wolters and Laffay[13] determined the focal length of the lens created by density variations within the external flow. The following parameters were used in their calculations:

$R' = 0.17$ m $\lambda_\infty = 10.6 \times 10^{-6}$ m

$R_C = 0.5$ m $\kappa'/\rho_\infty = 0.223 \times 10^{-3}$ m^3/kg

$M_\infty = 0.587$ $\theta' = 0$

altitude: 20,000 ft.

For these conditions a focal length of 18.2 km was determined. Since the distortion varies linearly with the ambient density, a fact which follows from equation (42), the focal length can be adjusted to sea level by an adjustment to density. For the same conditions as above except at sea level, the focal length would be 8.2 km. A value 8.2 km is consistent with results obtained in this report, 16.5 km.

Having compared in a rough way calculated results from references (12) and (13) with calculated results from this paper, the relative advantages and disadvantages of each model will now be compared. Reference (12) used $\partial I/\partial x$ and $\partial I/\partial y$ to predict tilt; $\partial^2 I/\partial x^2$ [see equation (54)] and

$\partial^2 I/\partial y^2$ were used to predict focal length. These were evaluated at the beam center. An analytical solution was obtained. Reference (12) also used a first order solution for the flow field, which is equation (16). This paper uses a second order solution as given by equation (41). Hence a more accurate flow field is used in this paper. Reference (12) yields a solution in simple form; this paper requires a desk top computer, eg. HP9830, or else a high degree of patience if a HP55 were to be used.

In contrast to reference (13) which used a numerical solution to the flow field, the second order analytical solution gives the flow field to any degree of spatial resolution required. Numerical solutions give results in discrete steps. Based on Figure 5 of reference (13) the ratio of step size to cylinder radius is 0.22. Figure 10 of this paper shows that approximately one-half of the phase distortion is generated in a step size 0.22. Of course a smaller step size can be used. Numerical techniques have the advantages of providing solutions for complex turret geometry. This paper is applicable only to a hemispherical turret.

Look at Figure 9 for which $\theta' = 90°$. The contours have a symmetry about the $\alpha = 0°$--$180°$ line and about the $\alpha = 90°$--$270°$ line. The phase distortion has positive values which give a negative lens. The focal length for $\alpha = 0°$ is considerably less than for $\alpha = 90°$. At $\theta' = 90°$, the beam is defocused.

It is apparent from Figures 4 to 9 that the phase distortion is a strong function of elevation angle θ'. Compensation for the phase distortion is possible, at least partially. However, the shape of the primary telescope mirror required for compensation is a function of both elevation angle and Mach number. Such compensation should fall within the capability of adaptive optics techniques.

To discuss the altitude dependence, recall $\kappa = \kappa' \rho_\infty / \rho_{SL}$. Both κ' and ρ_{SL} are constants for a given wavelength and specified atmospheric conditions. Consequently, κ varies directly with ρ_∞. Now examine equation (51). Since $\kappa << 1$, the term $1 + \kappa$ is essentially unity; it follows that $N-N_0$ varies directly as κ. Phase distortion changes as ρ_∞. Obviously as altitude increases, phase distortion decreases.

VIII. CONCLUDING REMARKS

Compressible flow over a sphere has been obtained forming the basis for a model of a blunt hemispherical laser turret. Phase distortion has been calculated for several freestream Mach numbers. Phase distortion data are presented for M_∞ equal to the critical Mach number. Calculations are consistent with those of references (12) and (13).

The phase distortion is a function of both elevation angle and Mach number. Hence optical compensation requires a variable shape primary mirror.

The model of a hemispherical laser turret provides insight to the behavior of phase distortion as a function of Mach number. See Figure 11. Also refer to Table III.

Another valuable aspect of the calculations is the decay of density perturbation with distance along the beam. See Figure 10. It is apparent that the distortion is fairly localized. Within a distance of $s/R = 1.0$, over 99% of the distortion occurs.

The formulation clearly shows the altitude dependence of phase distortion.

REFERENCES

1. L. M. Milne-Thompson, Theoretical Hydrodynamics, The MacMillan Co., New York, Fourth Edition, 1960.

2. Horace Lamb, Hydrodynamics, Dover Publications, New York, Sixth Edition, 1945.

3. Krishnamurthy Karamcheti, Principles of Ideal-Fluid Aerodynamics, John Wiley and Sons, New York, 1966.

4. Milton Van Dyke, Perturbation Methods in Fluid Mechanics, Parabolic Press, Stanford, California, 1975.

5. Hans W. Liepmann and Allen E. Puckett, Introduction to Aerodynamics of a Compressible Fluid, John Wiley and Sons, New York, 1947.

6. Klaus Oswatitsch, Gas Dynamics, Academic Press, New York, 1956.

7. Lord Rayleigh, "On the Flow of Compressible Fluid Past an Obstacle," The London, Edinburgh and Dublin Philosophical Magazine and Journal of Science, Sixth Series, Volume 32, No. 187, July 1916.

8. Tsuying Hsieh, "Hemisphere-Cylinder in Transonic Flow, M_∞ = 0.7-1.0," AIAA J., 13, pp. 1411-1413, 1975.

9. Tsuying Hsieh, "Hemisphere-Cylinder in Low Supersonic Flow," AIAA J., 13, pp. 1551-1552, 1975.

10. A. E. Fuhs and S. E. Fuhs, "Laser Beam Phase Distortion Due to Flow of Air Over the Telescope," Proceedings of Electo Optics/Laser Conference and Exposition, New York, September, 1976.

11. J. South, Jr., and A. Jameson, "Relaxation Solutions for Inviscid Axisymmetric Transonic Flow over Blunt or Pointed Bodies," Proceedings of the AIAA Computational Fluid Dynamics Conference, July 1973.

12. Richard J. Cook, "Aero-Optical Effect of the Inviscid Flow About a Sphere," Air Force Weapons Laboratory, unpublished manuscript, 1975.

13. D. J. Wolters and P. J. Laffay, "Mainstream Flow Effects on F-15 Turret Optics," McDonnell Aircraft Company Report MDC A3179, January 3, 1975.

DISTRIBUTION LIST

1.	Library Naval Postgraduate School Monterey, CA 93940	2
2.	Defense Documentation Cwnter Cameron Station Alexandria, VA 22314	2
3.	Professor Allen E. Fuhs, Code 69Fu Department of Mechanical Engineering Naval Postgraduate School Monterey, CA 93940	40
4.	Dean of Research Naval Postgraduate School Monterey, CA 93940	2
5.	PMS-405 Naval Sea Systems Command Washington, D. C. 20361	3
6.	Dr. W. Warren Aerospace Corporation El Segundo Boulevard El Segundo, CA 90245	1
7.	Naval Weapons Center Attn: Ron Dettling (Code 4581) China Lake, CA 93555	1
8.	Major Gregory Cannovan Defense Advanced Research Projects Agency 1400 Wilson Avenue Arlington, VA 22209	1
9.	Air Force Weapons Laboratory Attn: Major Keith Gilbert Kirtland Air Force Base, NM 87147	5
10.	Air Force Weapons Laboratory Attn: Dr. Barry Hogge Kirtland Air Force Base, NM 87147	1
11.	Institute for Defense Analyses Attn: Dr. Donald M. Dix 400 Army Navy Drive Arlington, VA 22202	1
12.	NASA Ames Research Center Attn: Mr. Thomas Gregory Moffett Field, CA 94035	1

13. Naval Air Systems Command
Attn: Mr. Ed Fisher AIR 350
Washington, D. C. 20361 — 1

14. LCDR Robert Spencer
Office of Test Director
Joint Services EO/GW CM Test Program
White Sands Missile Range, NM 88002 — 1

15. Naval Research Laboratory
Attn: Dr. John Hayes
Washington, D. C. 20375 — 1

16. Naval Research Laboratory
Attn: Dr. Ted Jacobs
Washington, D. C. 20375 — 1

17. Mr. V. Nikolashin
L.M.S.C.
P.O. Box 504
Bldg. 104, Dept. 62-04
Sunnyvale, CA 94088 — 1

18. Ben C. Platt
UDRI/LRE
Kirtland AFB, NM 87117 — 1

19. Air Force Weapons Laboratory
Attn: L. Sher
Kirtland Air Force Base, NM 87147 — 1

20. Air Force Weapons Laboratory
Attn: Col. D. T. Kyrazis
Kirtland Air Force Base, NM 87147 — 1

21. CAPT R. A. Massey
PM-22
Naval Sea Systems Command
Washington, D. C. 20362 — 1

22. Air Force Weapons Laboratory
Attn: CDR L. W. Brown
Kirtland Air force Base, NM 87147 — 1

23. C. D. Fawcett
ASD/XR2
Wright-Patterson Air Force Base, Ohio 45433 — 1

24. H. A. Hutchinson
ASD/ENS
Wright-Patterson Air Force Base, NM 87147 — 1

25. Air Force Weapons Laboratory
Attn: L. Wilson (ALC)
Kirtland Air Force Base, NM 87147 1

26. Air Force Weapons Laboratory
Attn: LCDR A. F. Schroeder (PGA)
Kirtland Air Force Base, NM 87147 1

27. Air Force Weapons Laboratory
Attn: Major B. D. O'Neil (LRO)
Kirtland Air Force Base, NM 87147 1

28. Air Force Weapons Laboratory
Attn: Paul H. Merritt (LRO)
Kirtland Air Force Base, NM 87147 1

29. Air Force Weapons Laboratory
Attn: Capt. R. V. Hemm (LRL)
Kirtland Air Force Base, NM 87147 1

30. Professor Stewart Collins
Ohio State University
190 North Oval Drive
Columbus, Ohio 43210 1

31. Professor William Meecham
University of California, Los Angeles
Los Angeles, CA 90024 1

32. Professor Abraham Hertzberg
University of Washington
Seattle, WA 98195 1

33. Zentralstelle für Luft-U. Raumfahrtdokumentation
u. - information (ZLDI)
Postfach 860 880
D-8000 Munchen 86 1

34. Mr. Donald DeCoursey
Science Applications
1651 Old Meadows Rd., Suite 620
McLean, VA 22101 1

35. Professor Fred Culick
Division of Engineering and Applied Science
California Institute of Technology
Pasadena, CA 91125 1

36. Dr. Garret Vanderplaats (Code 69Vd)
Department of Mechanical Engineering
Naval Postgraduate School
Monterey, CA 93940 1

37. NASA/Ames Research Center
Attn: Captain John Otton, USAF
Moffett Field, CA 94035 1